Novel Mechanisms of Strigolactone-Induced DWARF14 Degradation in *Arabidopsis thaliana*

Elena Sánchez Martín-Fontecha[1,5,6], Francesca Cardinale[2], Marco Bürger[3], Cristina Prandi[4], Pilar Cubas[1,#]

1. Plant Molecular Genetics Department, Centro Nacional de Biotecnología-CSIC, Campus Universidad Autónoma de Madrid, 28049, Madrid, Spain
2. Dipartimento di Scienze Agrarie, Forestali e Alimentari, Università di Torino, Largo Braccini 2, 10095, Grugliasco, Italy
3. Plant Biology Laboratory, Salk Institute for Biological Studies, La Jolla, CA 92037, USA
4. Dipartimento di Chimica, Università degli Studi di Torino, Via P. Giuria 7, I-10125, Torino, Italy
5. Current address: Department of Plant Biotechnology and Bioinformatics, Ghent University, 9052, Ghent, Belgium
6. Current address: Vlaams Instituut voor Biotechnologie (VIB)-Center for Plant Systems Biology, 9052, Ghent, Belgium

#Corresponding author: pcubas@cnb.csic.es

Running head: SL-induced D14 degradation

Keywords: DWARF14, Strigolactone perception, Strigolactone signalling, proteasomal degradation.

Abstract

Strigolactones (SLs) are carotenoid-derived compounds that regulate various aspects of plant development, physiological responses and plant interactions with microorganisms. In angiosperms, the SL receptor is the α/β hydrolase D14 that, upon SL binding, undergoes conformational changes, triggers SL-dependent responses and hydrolyses SLs. Arabidopsis SL signalling involves the formation of a complex between SL-bound D14, the E3-ubiquitin ligase SCF^{MAX2} and the transcriptional corepressors SMXL6/7/8 (SMXLs), which become ubiquitinated and degraded by the proteasome. However, the sequence of events that result in SL signalling and the requirement of SL hydrolysis for this process remain unclear. In addition, SL destabilises the D14 receptor. The biological significance of SL-induced D14 degradation is unclear, although it has been proposed to create a negative feedback loop in SL signalling. The current model proposes that D14 degradation occurs after SMXLs ubiquitination and proteolysis, via the same E3-ubiquitin ligase that targets the repressors.

In this work we quantitatively studied the degradation dynamics of Arabidopsis D14 in response to SLs *in planta*. For this, we conducted fluorescence and luminescence assays to monitor D14 stability dynamics upon SL treatments, in transgenic lines expressing *D14* fused to *GREEN FLUORESCENT PROTEIN* (*GFP*) or *LUCIFERASE* (*LUC*), in wild-type and SL-signalling mutant backgrounds. Mutant D14 proteins predicted to be non-functional for SL signalling were also examined, and their capability to bind SLs *in vitro* was studied using Differential Scanning Fluorimetry (DSF). Finally, we used a non-hydrolysable SL to test the requirements of SL hydrolysis for D14 and SMXL7 degradation. Our research revealed that SL-induced D14 degradation may occur in the absence of SCF^{MAX2} and/or SMXLs by a proteasome-independent mechanism. Additionally, we observed conditions in which the efficiency of SL-induced degradation of D14 is not aligned with that of SMXL7 degradation. Finally, our results indicate that the hydrolysis of SLs is not a prerequisite to trigger either D14 or SMXL7 degradation. These findings suggest the existence of a regulatory mechanism governing D14 degradation more complex than anticipated, and provide novel insights into the dynamics of SL signalling in Arabidopsis.

Introduction

Strigolactones (SLs) are a class of carotenoid-derived compounds (Al-Babili and Bouwmeester, 2015) known to act as exuded and endogenous signals in both beneficial and detrimental interactions with (micro)organisms in the rhizosphere (Akiyama *et al.*, 2005; Besserer *et al.*,

2006). They also play crucial roles in the control of plant development and growth: they are inhibitors of bud outgrowth and shoot branching, and regulators of internode elongation, height, stem secondary growth, leaf development and senescence, reproduction and of root architecture (reviewed in Rameau *et al.*, 2019; Dun *et al*., 2023; Guercio *et al*., 2023). SLs are mediators of physiological and morphological responses to water and nutrient deprivation, including the ability to form mycorrhizae and nodules, and are important for full antioxidant capacity in response to stress (reviewed by Trasoletti *et al.*, 2022; Lanfranco *et al.*, 2018). Their perception is repressed by sugars and citrate, that may act as proxies for the plant nutritional status (Tal *et al*., 2022; reviewed by Barbier *et al.*, 2023). Thus, they are thought to integrate environmental signals with plant plasticity and physiological acclimation.

Structurally, SLs are tricyclic lactones (ABC tricyclic system) connected to a butenolide (D-ring) through an enol-ether bond (reviewed by Dun *et al.*, 2023). There are two key stereochemical centres in these molecules, one at the junction of the B and C rings, and the other at the junction of the D-ring. The first stereocentre is not critical in defining SL activity, but does divide SLs into two subclasses, the 5-deoxystrigol (5DS) and 4-deoxyorobanchol (4DO) types. Naturally occurring plant SLs display a 2´R configuration of the D-ring (reviewed in Yoneyama *et al.*, 2018), which is required for their biological activity.

The signalling mechanism of SLs is based on a hormone-induced proteolysis pathway similar to that of other plant hormones such as auxins, gibberellins and jasmonate. It involves a hormone receptor, and a Skp1-Cullin-F-box (SCF) E3-ubiquitin ligase complex that targets specific protein substrates for polyubiquitination and subsequent degradation by the 26S proteasome (Blázquez *et al.*, 2020). In angiosperms, the SL receptor is the α/β hydrolase D14, unusual insofar as it can hydrolyse its ligand, albeit at a low turnover rate. D14 contains a hydrophobic binding pocket that can directly bind to the SL molecule (reviewed in Barbier *et al.,* 2023; Guercio *et al.,* 2023). The protein active site is located at the bottom of the SL binding pocket and is formed by a conserved catalytic triad, serine-histidine-aspartic acid (S97-H247-D218 in Arabidopsis).

SL signalling is initiated with the binding of SLs to D14. The nucleophilic attack of C5´of SL by the catalytic serine is followed by several states involving intermediates that may affect the enzymatic activity of D14 (reviewed in Guercio *et al.,* 2023). SL signalling also requires the formation of a complex between SL-D14, the E3-ubiquitin ligase complex $SCF^{MAX2/D3}$, which confers the substrate specificity by the F-box protein MORE AXILLARY GROWTH2 (MAX2) or D3 (in Arabidopsis and rice respectively, Ryun Woo *et al.*, 2001; Stirnberg *et al.*, 2002, 2007; Ishikawa *et al.*, 2005; Johnson *et al.*, 2006), and the transcriptional corepressors SUPPRESSOR OF MAX2-1-LIKE (SMXL)6, SMXL7 and SMXL8 (hereafter SMXLs) or DWARF53 (D53) in Arabidopsis or rice respectively (Jiang *et al.*, 2013; Zhou *et al.*, 2013; Soundappan *et al.*, 2015;

94 Wang *et al.*, 2015; Liang *et al.*, 2016). SMXLs/D53 are targets for polyubiquitination by $SCF^{MAX2/D3}$
95 and proteasomal degradation, which elicits SL-dependent gene expression (Jiang *et al.*, 2013;
96 Zhou *et al.*, 2013; Soundappan *et al.*, 2015; Wang *et al.*, 2015; Liang *et al.*, 2016). To date, the
97 sequence of events leading to complex formation and whether SL hydrolysis is required for this
98 process are yet unclear.
99 The formation of the complex and the subsequent SL signalling requires SL-induced
100 conformational changes in D14. One model, based on structural data, proposes that SL
101 hydrolysis is essential for these conformational changes (Yao *et al.,* 2016; Saint Germain *et al.*,
102 2016). A second model, based on time-course analyses of SL binding and hydrolysis and genetic
103 data, proposes that the intact SL molecule triggers complex formation and signalling. This model
104 is further supported by the observation that the recruitment of D3 and D53 requires a pre-
105 hydrolysis state of D14-SL (Shabek *et al.,* 2018; Seto *et al.,* 2019). In this model, hydrolysis of SLs
106 would serve to deactivate the bioactive form of the hormone (Seto *et al.,* 2019). Nevertheless,
107 the exact series of events, or whether ligand hydrolysis is indeed required for SL signalling, is not
108 settled yet. Furthermore, D14 may not be a single turnover enzyme, as the interaction between
109 the hydrolysis intermediate and D14 seems to be reversible. This implies that the receptor could
110 be reused and participate in several SL perception/deactivation cycles (Shabek *et al.*, 2018).
111 After SL-induced ubiquitination and degradation of the SMXLs/D53, the SL receptor D14 is itself
112 destabilised in the presence of SLs. This suggests that SLs may promote a negative feedback loop
113 within the SL signalling cascade, by limiting the availability of receptors and thus modulating the
114 sensitivity to SLs (Chevalier *et al.*, 2014). Evidence for the phenomenon of SL-induced
115 destabilisation of D14 has been found in Arabidopsis and rice. Arabidopsis transgenic lines
116 expressing translational fusions of *D14* and *GREEN FLUORESCENT PROTEIN* (*GFP*) or *β-*
117 *GLUCURONIDASE* (*GUS*) coding sequences (CDS) display a significant decrease in D14:GFP and
118 D14:GUS protein levels, respectively, following treatments with SLs (Chevalier *et al.*, 2014). Cell-
119 free degradation assays using Arabidopsis plant extracts and a purified D14:HA protein show
120 reduced D14:HA protein abundance when exposed to SLs (Tal *et al.*, 2022). Rice *D14:GFP*- and
121 *HA:D14*-expressing calli display D14:GFP and HA:D14 destabilisation after addition of SLs (Hu *et*
122 *al.,* 2017; Patil *et al.,* 2022).
123 The initially proposed model for D14 degradation hypothesises that, following ubiquitination
124 and proteasomal removal of SMXLs/D53, D14 becomes accessible to ubiquitination and
125 proteasomal degradation by the same $SCF^{MAX2/D3}$ complex (Chevalier *et al.*, 2014; Hu *et al.*, 2017;
126 Tal *et al.*, 2022). Several observations support this scenario: SL treatments induce ubiquitination
127 of D14:GFP in rice (Hu *et al.*, 2017); degradation of Arabidopsis and rice D14:GFP can be reduced
128 by proteasome inhibitors (Chevalier *et al.*, 2014; Hu *et al.*, 2017); destabilisation of D14:GFP is

129 decreased in Arabidopsis *max2* and rice *d3* mutants (Chevalier *et al.*, 2014; Hu *et al.*, 2017).
130 Moreover, rice SL-insensitive *d53* mutants render D14:GFP resistant to SL-induced degradation,
131 which led to propose that D14 and D53 degradation are coupled, and that both are strongly
132 associated to the SL signalling status (Hu *et al.*, 2017). Finally, D14 mutant analyses suggest that
133 SL hydrolysis is essential for D14 degradation (Hu *et al.*, 2017).
134 This general model is derived from the amalgamation of a wide array of heterogeneous sources,
135 most of them involving callus cultures and cell-free assays performed mainly in rice. Therefore,
136 it remains largely untested *in planta* whether MAX2 and SMXLs are indispensable for the full
137 extent of SL-induced D14 degradation in Arabidopsis. Moreover, the biological significance of
138 the SL-induced D14 degradation and its relationship with SL signalling remains unclear.
139 In this work we systematically studied, quantitatively and *in planta,* the degradation dynamics
140 of the Arabidopsis D14 protein (AtD14, hereafter D14) in response to SLs. With this aim we
141 generated transgenic lines constitutively expressing the *D14* CDS fused to that of the *GFP* or
142 *LUCIFERASE (LUC)*, in wild-type and mutant backgrounds affected in the SL signalling machinery.
143 We then measured D14:GFP fluorescence signal (using time-lapse fluorescence quantitative
144 microphotography) or D14:LUC activity (using luminescence assays) in plants treated with the
145 synthetic SL analogue $GR24^{5DS}$. We performed similar assays with D14 proteins with mutations
146 in residues thought to be critical for D14 activity or for interaction with other components of the
147 SL signalling machinery. The ability of these mutants to bind SLs was tested by Differential
148 Scanning Fluorimetry (DSF). Additionally, we used synthetic, non-hydrolysable SL derivatives to
149 assess the requirement for SL hydrolysis during this process.
150 Our results reveal novel and unexpected features of D14 degradation in Arabidopsis that are
151 inconsistent with the current models being exclusive. We show that SL hydrolysis upon binding
152 to D14 is not essential for the degradation of the receptor. We also found indications of a
153 proteasome-independent mechanism of D14 degradation and provided compelling evidence
154 that neither MAX2 nor the SMXLs are strictly essential for D14 degradation, although they do
155 contribute to the process. Finally, we report cases in which the efficiency of SL-induced D14
156 degradation is largely divergent from that of SMXL7. All these results indicate that, in addition
157 to the SCF^{MAX2}/SMXLs-associated mode of D14 degradation, there are alternative pathways to
158 modulate D14 levels in the presence of SLs.
159
160 **Material and Methods**
161 *Plant material*
162 Wild-type *Arabidopsis thaliana* plants of the Columbia-0 (Col-0) ecotype were used. The *d14-1*
163 mutant (Arite *et al.*, 2009; Waters *et al.*, 2012), was obtained from the Nottingham Arabidopsis

164 Stock Centre (NASC ID:N913109). The *max2-1* mutant (Stirnberg *et al.*, 2002) was provided by
165 Dr. Ottoline Leyser. T-DNA insertional lines *smxl6-4 smxl7-3 smxl8-1* (*s678*) and *smxl6-4 smxl7-3*
166 *smxl8-1 max2-1* (*s678m*) (Liang *et al.*, 2016) were provided by Dr. Tom Bennett. Experiments
167 were performed in homozygous lines, except for the SMXL7:LUC degradation assays in
168 *35S:D14^{P169L}:GFP;d14-1 and 35S:D14^{G158E}:GFP;d14-1* background that were performed in F1
169 hemizygous lines from crosses of these lines with *UB:SMXL7:LUC;d14-1.*
170
171 *Growth conditions*
172 Arabidopsis seeds were sown in trays containing a mix of commercial soil and vermiculite (3:1
173 proportion), stratified in darkness 2-3 days at 4 °C and grown in long day conditions (16 h light/8
174 h dark). Humidity rate was 60%, temperature 22 °C and white light (photosynthetically active
175 radiation, 100 $\mu mol \cdot m^{-2} s^{-1}$) was provided by cool-white 20- W F20T12/CW tubes (Phillips). For
176 *in vitro* studies, seeds were surface-sterilised by 7 min incubation in 70% bleach (v/v) and 0.01%
177 (v/v) Tween-20, sown in Murashige and Skoog (MS) with 1% (w/v) sucrose and either 1.2% (w/v)
178 agar (vertical plates) or 0.7% (w/v) agar (horizontal plates). Seeds were stratified as above, and
179 grown in 16 h light/8 h dark photoperiod at 22 °C.
180
181 *Phenotypic analysis of adult plants*
182 Primary rosette branches (RI) and rosette leaves (RL) were counted 2 weeks after bolting of the
183 main inflorescence. Only branches longer than 0.5 cm were quantified. To avoid variations due
184 to flowering time (number of nodes and axillary meristems) in all experiments, branching was
185 defined as the ratio between RI/RL. Plant height was determined 2 weeks after bolting, as the
186 distance between the rosette and the apex of the main inflorescence. The position of plants
187 within the growing trays was randomised to minimise environmental variation.
188
189 *Constructs*
190 All plasmids were generated using Gateway technology (Invitrogen, Life Technologies). pDONR
191 vectors carrying the CDS of *D14* and *SMXL7* were recombined with pDEST plasmids to generate
192 binary vectors by LR Clonase reactions. For *35S Cauliflower Mosaic Virus Promoter*
193 (*35S):D14:GFP* constructs we used the destination vector pGWB505 (Nakagawa *et al.*, 2007) and
194 for MultiSite Gateway Technology constructs we used pB7M34GW (Karimi *et al.*, 2005). pAB118
195 and pAB119 were used for *LexA:CDS:mCherry* and *LexA:CDS:mCherry:GFP* constructs
196 (Bleckmann *et al.*, 2010). The CDS of *D14^{H247A}* and *D14^{G158E}* mutants (Yao *et al.*, 2016) were
197 provided by Dr. Ruifeng Yao. Primers used are listed in Supplemental Table 1.
198

199
200
201
202 *Generation of transgenic lines*
203 Binary vectors were transformed into the *Agrobacterium tumefaciens* strain AGL-0. Transgenic
204 Arabidopsis plants were generated by agroinfiltration using the floral dip method (Clough and
205 Bent, 1998).
206
207 *LUC activity assays*
208 LUC assays were performed as described (Sánchez *et al.*, 2018; Sánchez *et al.*, 2021). Briefly, 6
209 days post germination (dpg), *LUC*-expressing seedlings were placed facing up in MS-containing
210 96-wells plates. D-luciferin substrate (Sigma) was added to each well to a final concentration of
211 10 µM, and plates were pre-incubated for 2-3 h before treatment. LUC activity (counts per
212 second, cps) was measured using a LB 960 microplate luminometer centre system (Berthold
213 Technologies) with MikronWin 2000 software under controlled temperature (22 ^{o}C). LUC activity
214 was measured (2 s counting time) every 10-15 min for 16 h. The LUC activity variation over time
215 was calculated as a percentage of the t=0 signal for each plant. Then, we obtained the mean LUC
216 activity of each treatment/genotype and represented the Relative LUC units of each
217 treatment/genotype normalised to the mean of its mock treatment values at each time point.
218 Experiments were performed at least twice (for n>6) or three times (for n<6).
219
220 *Time-lapse fluorescence microphotography*
221 D14:GFP degradation assays were performed as described (Li *et al.*, 2022) with 4-dpg *GFP*-
222 expressing seedlings. Plants were treated with 5 µM GR24^{5DS} (StrigoLab) and equivalent volumes
223 of acetone were added for mock controls. When proteasome inhibitors were used, seedlings
224 were pre-incubated with 50 µM MG132 (PeptaNova) and 20 nM epoxomicin for 1 h before SL
225 addition, and fresh inhibitor was added together with the hormone. Images were captured every
226 15-20 min for 16 h with a Microfluor Leica DMI6000B fluorescence microscope using a 10X
227 objective and 470 nm light. Videos were obtained by Z projection with the Maximum Intensity
228 method using the Leica Application Suite Advanced Fluorescence software (LAS-AF). GFP signal
229 was quantified with Fiji (Schindelin *et al.*, 2012) using Region of Interest (ROI) Multi Measure
230 plugging after determining a threshold range to eliminate the background. The GFP signal
231 variation over time was calculated as in the LUC activity assays. Each experiment was performed
232 at least twice, with 3-4 seedlings analysed per treatment.
233

234 *Quantitative analysis of protein degradation dynamics*

235 We defined protein half-life as the time at which plants displayed a value of LUC activity or GFP
236 signal of 50% of that at t=0 h. When protein degradation did not reach values of 50% at the end
237 of the assay, and therefore half-life could not be calculated, the half-life was depicted with
238 symbols clipped at the edge of the y axis. We defined the endpoint signal as the LUC activity (%)
239 or GFP signal (%) of each plant at the end of the assay (t=16 h for D14:GFP; t=15 h for D14:LUC;
240 t=3 h for SMXL7:LUC) normalised to the mean of the mock treatment values.

241

242 *D14 degradation assays by immunoblot*

243 Seven-dpg seedlings grown horizontally *in vitro* were transferred to multiwell plates with liquid
244 MS 1% (w/v) sucrose supplemented with 5 µM $GR24^{5DS}$, or an equivalent volume of acetone as
245 mock control, and incubated for 8 h at 22 °C. When necessary, plants were pre-treated for 1 h
246 with the proteasome inhibitors 50 µM MG132 (PeptaNova) and 20 nM epoxomicin. Fresh
247 inhibitor was added together with $GR24^{5DS}$. After treatment, seedlings were collected and frozen
248 in liquid N_2 for protein extraction and immunodetection. Protein was extracted in 50 mM Tris-
249 HCl pH 7.5, 150 mM NaCl, 0.1% NP-40, 1 mM PMSF and protease inhibitor mix (Roche).
250 Protein extracts were denatured in 5X loading buffer (1 M Tris-HCl pH 6.8, 25% (v/v) glycerol,
251 8% (w/v) SDS, 200 µg/ml Bromophenol Blue and 10% (v/v) β-mercaptoethanol). Samples were
252 separated by SDS-PAGE. Proteins were transferred to a polyvinylidene difluoride (PVDF)
253 membrane (Millipore) and probed with α-GFP-HRP antibody (1:1000, Milteny Biotec), α-
254 ubiquitin (1:500, Enzo Life Sciences) or α-actin (1:1000, Abcam). Signal was detected using the
255 ECL Prime Western Blotting Detection Reagent (Amersham).

256

257 *Affinity purification of ubiquitinated proteins*

258 Seven-dpg seedlings grown horizontally in MS medium were pre-treated with the proteasome
259 inhibitors 50 µM MG132 and 20 nM epoxomicin for 1 h and then with 10 µM $GR24^{rac}$ (Strigolab)
260 for further 3 h at 22ºC. Seedlings were then frozen in liquid N_2 and proteins were extracted using
261 buffer BI (50 mM Tris-HCl pH 7.5, 20 mM NaCl, 0.1% Nonidet P-40, 5 mM ATP) plus the Protease
262 inhibitor cocktail (Roche), 1 mM PMSF, 50 µM MG132, 10 nM Ub aldehyde (Enzo Life Sciences),
263 10 mM N-ethylmaleimide and 5 µM $GR24^{rac}$. Protein extracts were incubated with 20 µL of
264 prewashed p62 agarose (Enzo Life Sciences) or amylose resin (negative control; New England
265 Biolabs) at 4°C for 3 h. The beads were washed twice with BI buffer and once with BI buffer
266 supplemented with 200 mM NaCl. Proteins were eluted by boiling in 5X loading buffer and
267 separated by SDS-PAGE. D14:GFP and total ubiquitinated proteins were detected by
268 immunoblotting with α-GFP-HRP or α -ubiquitin respectively. Signal was detected using the ECL

269 Prime Western Blotting Detection Reagent (Amersham) or SuperSignalTM West Femto
270 Maximum Sensitivity Substrate (Thermo Fisher).
271
272 *Förster Resonance Energy Transfer-acceptor photobleaching (FRET-APB) assay*
273 Leaves of 3-4-week-old *Nicotiana benthamiana* plants were agroinfiltrated and sprayed with 10
274 µM estradiol (Sigma) 24 h after infiltration to induce protein expression. FRET-APB assays were
275 performed 24 h after estradiol induction on a Leica TCS SP5 laser scanning confocal microscope
276 with a 63x/1.2NA water immersion objective as described (Nicolas *et al.*, 2015). The FRET-APB
277 wizard of LAS-AF was used with the following parameters: acquisition speed 700 Hz; pinhole
278 60.7 µm; image format 512x512 pixels; zoom 6X. ROIs of 6x3.5 µm were photobleached with 10
279 repeated exposures (laser 561 nm, 100% power level). Images were processed using LAS-AF
280 Software. FRET Efficiency (E_{FRET}%) was measured as the increase of donor (GFP) fluorescence
281 intensity after photobleaching of the acceptor (mCherry).
282
283 *Differential Scanning Fluorimetry*
284 Protein production in *E. coli* and DSF assays were performed as previously described (Bürger *et*
285 *al.*, 2019).
286
287 *Statistical analyses and bioinformatics methods*
288 R version 3.5.3 (http://www.R-project.org/; The R Development Core Team, Preprint) and the
289 Rcmdr package version 2.5.2 (Fox, 2005) were used for the statistical analyses. Comparisons
290 between control and treatments were analysed by one-way ANOVA and Tukey's test with
291 Welch´s correction for unequal variances. Different letters denote statistical differences ($p <$
292 0.05). GraphPad Prism Software v. 8.3 for Windows (San Diego, California USA,
293 www.graphpad.com) was used for data representation. The PyMOL Molecular Graphics System
294 (Schrödinger, LLC.; https://pymol.org/) was used for molecular visualisations of 3D protein
295 structures.
296
297 **Results**
298 *Quantitative assays to study D14 degradation dynamics*
299 Studies in both Arabidopsis and rice have shown that D14 is destabilised in the presence of SLs
300 (Chevalier *et al.*, 2014; Hu *et al.*, 2017; Tal *et al.*, 2022). To study more in detail the dynamics of
301 D14 degradation, we generated *35S:D14:GFP* and *UB:D14:LUC* transgenic lines that allowed us
302 to perform quantitative assays *in vivo*. Quantification of the GFP signal using time-lapse
303 fluorescence quantitative microphotography, and LUC activity using luminescence assays could

304 be correlated with D14 levels at different time points. We selected *35S:D14:GFP* and
305 *UB:D14:LUC* lines that completely rescued the increased branching phenotypes of knock-out
306 *d14-1* mutants (Supplemental Fig. 1A, B, K) and almost completely rescued the phenotype of
307 reduced height (Supplemental Fig. 1F, G, K).
308 Next, we performed time-lapse fluorescence and luminescence assays to analyse, quantitatively
309 and *in planta,* the SL-induced destabilisation of D14:GFP and D14:LUC, respectively (Fig. 1,
310 Supplemental Fig. 2, 3, Supplemental files S1, S2). We used as reference values the protein half-
311 life (Fig. 1B, F) and endpoint LUC or GFP signal (Fig. 1C, G). The protein half-life of D14:GFP and
312 D14:LUC was of 3-8 h in plants treated with 5 µM $GR24^{5DS}$ (Fig. 1A, B, D, F). However, we
313 observed that the degradation dynamics of D14:GFP in roots and hypocotyls (which could be
314 measured separately in the *35S:D14:GFP* lines) was not identical: D14:GFP was degraded faster
315 (shorter half-life) and more completely (lower end-point signal) in hypocotyls than in roots (Fig.
316 1A-C).
317 We assayed the D14:LUC activity with concentrations of $GR24^{5DS}$ ranging from 100 nM to 20 µM,
318 and found that the protein was destabilised in a dose-dependent manner between 100 nM and
319 1-5 µM $GR24^{5DS}$, concentrations at which the shortest half-life and most complete degradation
320 (lowest endpoint LUC signal) were observed. Higher hormone concentrations did not lead to
321 faster or more complete D14:LUC degradation (Fig. 1D-G). In general, the dynamics of
322 degradation were not significantly different in the wild type and in *d14-1* mutant backgrounds
323 either for D14:GFP (Fig. 1A-C) or for D14:LUC (Fig. 1D-G).
324
325 *Degradation of D14:GFP is only partly mediated by the 26S proteasome*
326 Previous studies have suggested that the proteasome is the pathway for D14 destabilisation.
327 (Chevalier *et al.*, 2014; Hu *et al.*, 2017). Proteins targeted for proteasomal degradation are
328 polyubiquitinated for recognition by the proteasome machinery. To test whether D14:GFP was
329 ubiquitinated upon SL treatment in Arabidopsis, we treated 7-dpg *35S:D14:GFP* seedlings with
330 GR24, affinity-purified ubiquitinated proteins from their extracts using a Ubiquitin (Ub)-binding
331 resin, and performed α-GFP immunoblots. We detected D14:GFP and higher molecular weight
332 bands corresponding to different D14:GFP poly-ubiquitinated forms (Ub(n):D14:GFP; Fig. 2A).
333 This result confirmed that, like rice D14, Arabidopsis D14:GFP is polyubiquitinated in the
334 presence of exogenous SLs in Arabidopsis.
335 It has been reported that SL-induced D14 degradation can be suppressed by treatments with
336 the 26S proteasome inhibitor MG132 (Chevalier *et al.*, 2014; Hu *et al.*, 2017). To confirm this,
337 we performed immunoblots with 7-dpg *35S:D14:GFP* seedlings treated with $GR24^{5DS}$ both with
338 and without proteasome inhibitors (MG132 and epoxomicin). Plants treated with $GR24^{5DS}$ and

339 proteasome inhibitors displayed higher levels of D14:GFP than those without inhibitors, but
340 some degradation of D14:GFP was still evident when compared to plants not treated with
341 GR24^{5DS} (Fig. 2B). Moreover, time-lapse fluorescence microphotography seemed to indicate
342 that the D14:GFP degradation dynamics are delayed, but not abolished by the inhibitors (Fig.
343 3A, B), and that the half-life (Fig. 3F) and endpoint signal (Fig. 3G) parameters did not always
344 capture significant differences between treated and untreated plants. These results point to the
345 existence of a proteasome-independent mechanism contributing to D14:GFP degradation along
346 with the proteasome-dependent pathway.
347
348 *The strigolactone signalling complex SCF^{MAX2} contributes to, but is not essential for D14*
349 *degradation*
350 Previous studies have shown that SL-induced D14 degradation is largely compromised in *max2*
351 mutants (Chevalier *et al.*, 2014; Hu *et al.*, 2017), suggesting that the SCF^{MAX2} complex is pivotal
352 in this process. Therefore, we quantitatively investigated the role of *MAX2* in more detail, by
353 performing D14:GFP stability assays in *35S:D14:GFP;max2-1* lines. Remarkably, we found that,
354 in *max2* mutants, there was still a certain level of D14:GFP degradation induced by GR24^{5DS},
355 although reduced as compared to the degradation observed in the wild type. This degradation
356 was largely unaffected by proteasomal inhibitors (Fig. 3C, F, G). We further confirmed these
357 results by LUC assays performed in *UB:D14:LUC;max2-1* (Fig. 3H-J).
358 As a complementary approach, we analysed, in SL-treated plants, the stability of two D14
359 mutant proteins whose capability to interact with MAX2 is compromised due to amino acid
360 substitutions at the lid domain, a region involved in the D14-MAX2 interaction. One of these
361 proteins was D14^{G158E} (Supplemental Fig. 4A, B), unable to interact with the MAX2 rice ortholog
362 D3 in pull-down assays (Yao *et al.*, 2016). In *35S:D14^{G158E}:GFP;d14-1* transgenic lines treated with
363 GR24^{5DS}, we detected a significant although not complete degradation of D14^{G158E}:GFP, similar
364 to that observed in *max2* mutants, and also insensitive to proteasome inhibitors (Fig. 3D, F, G).
365 DSF assays with increasing concentrations of GR24 indicated that D14^{G158E} gets destabilised only
366 at much higher concentrations of GR24^{5DS} than wild-type D14 (Supplemental Fig. 5A, B), which
367 may explain the suboptimal degradation of the protein.
368 Next we analysed the SL-induced proteolysis of D14^{P169L}:GFP, another mutant protein with an
369 amino acid substitution colocalizing with the area of D14-MAX2 interaction on the external
370 surface of the lid domain (Chevalier et al., 2014; Yao et al., 2016; Supplemental Fig. 4C, D). In
371 *35S:D14^{P169L}:GFP;d14-1* transgenic lines, we detected a fast and significant protein degradation
372 in response to GR24^{5DS}, insensitive to proteasome inhibitors (Fig. 3E-G; Li *et al.*, 2022). These
373 degradation patterns were indistinguishable in wild-type and in *max2* mutant backgrounds

374 (*35S:D14^{P169L}:GFP;max2-1*) (Supplemental Fig. 6A-C), consistently with a lack of interaction of
375 D14^{P169L} with MAX2.
376 All these results suggest that SLs can still promote the degradation of D14 in the absence of an
377 interaction with MAX2. This degradation may occur through a mechanism independent of the
378 proteasome.
379
380 *The interaction of D14 with the SL signalling repressors SMXL6, SMXL7 and SMXL8 contributes*
381 *to, but is not essential for D14 degradation*
382 In the presence of SLs, the SMXLs are rapidly recruited to the SL-D14-SCF^{MAX2} complex and
383 targeted for proteasomal degradation. We assessed whether this was a prerequisite for D14
384 destabilisation by performing D14:LUC degradation assays in the triple mutant *smxl6-4 smxl7-3*
385 *smxl8-1* (*s678)* (*UB:D14:LUC;s678* lines). D14:LUC was destabilised in the *s678* mutant
386 background with degradation dynamics almost identical to those observed in wild type (Fig. 4A-
387 C). This indicates that these SMXLs are not essential for SL-induced D14 degradation. To assess
388 whether the SMXLs-independent D14 degradation occurred via SCF^{MAX2}, we studied D14:LUC
389 degradation in the quadruple mutant *s678;max2-1* (*UB:D14:LUC;s678;max2*). In *s678;max2*,
390 D14:LUC half-life was longer than in wild type or *s678* but shorter than in *max2-1* (Fig. 4A-C).
391 This may indicate that, in the absence of the SMXLs, D14 degradation can still occur both *via* the
392 faster SCF^{MAX2} pathway (*s678*) or via a slower MAX2-independent pathway (*s678;max2*).
393 Furthermore, the observation that in *max2* mutants D14:LUC half-life is longer than in
394 *s678;max2* suggests that the interaction of the SMXLs with SL-D14 may interfere with the MAX2-
395 independent pathway of D14 degradation, perhaps by making D14 less accessible to the
396 alternative proteolytic machinery.
397
398 *Relationship between D14 and SMXL7 degradation patterns and SL signalling status*
399 Next, we investigated whether the extent of D14 degradation was strongly associated with
400 SMXL7 degradation and SL signalling in Arabidopsis. For this we used *UB:SMXL7:LUC* transgenic
401 lines that we combined with *d14-1* and *max2-1* mutants and with *D14:GFP*-expressing transgenic
402 lines.
403 First, we confirmed that SMXL7:LUC degradation was strictly dependent on D14, the only
404 reported SL receptor in Arabidopsis. Indeed, *d14-1* mutants displayed no degradation of
405 SMXL7:LUC upon GR24^{5DS} treatment (Fig. 5A-C). This contrasted with the efficient destabilisation
406 of D14:LUC in *s678* mutants (see above, Fig. 4A).
407 Next, we studied whether there was a correlation between the SL-induced degradation of
408 D14:GFP/LUC and that of SMXL7:LUC in several conditions and genetic backgrounds analysed in

409 this work. In general, SMXL7 degradation efficiency paralleled that of D14. SMXL7:LUC was
410 destabilised by GR24^{5DS} in a dose-dependent manner (Fig. 5D-F) although at much lower SL
411 concentrations than D14 (Fig. 1D, E). Also, the partial degradation of D14 in *max2-1* (Fig. 3C, H)
412 was mirrored by a partial degradation of SMXL7:LUC (*UB:SMXL7:LUC;max2-1* lines) (Fig. 5A-C)
413 supporting the possibility that SMXL7:LUC can also be targeted from degradation upon
414 interaction with SL-D14 in the absence of MAX2.
415 However, in certain scenarios, the efficiency of SL-induced degradation of D14 and SMXL7 were
416 largely different. For instance, we showed a noticeable but very reduced degradation of
417 D14^{G158E}:GFP as compared to D14:GFP (Fig. 3D, F, G). We combined *UB:SMXL7:LUC;d14-1* with
418 *35S:D14^{G158E}:GFP;d14-1* and studied SMXL7:LUC degradation in the F1
419 (*35S:D14^{G158E}:GFP/+;UB:SMXL7:LUC/+;d14-1*). These plants were in a *d14-1* mutant background,
420 in which SMXL7:LUC could only interact with D14^{G158E}:GFP. Remarkably, SMXL7:LUC displayed a
421 fast and efficient degradation indistinguishable from that in the wild type, in which SMXL7:LUC
422 interacts with a wild-type D14 (Fig. 5A-C). Conversely, although D14^{P196L}:GFP degradation was
423 slightly faster than that of D14:GFP (Figure 3E-G), the SMXL7:LUC degradation in
424 *35S:D14^{P169L}:GFP/+; UB:SMXL7:LUC/+*; *d14-1* was significantly less efficient than in the wild-type
425 background (Fig. 5A-C). These results indicate that the degradation of the repressor of the SL
426 pathway SMXL7 and that of the receptor D14 are not necessarily correlated in a quantitative
427 manner.
428 Moreover, D14 degradation efficiency was not consistently aligned with the status of SL
429 signalling, as measured by the phenotype of the lines studied. For example, despite the
430 inefficient degradation of D14^{G158E}:GFP, the *35S:D14^{G158E}:GFP;d14-1* lines had an almost wild-
431 type branching and height phenotypes (Supplemental Fig. 1D, I, K) in agreement with the wild-
432 type SMXL7:LUC degradation patterns (Fig. 5D-F). In contrast, although D14^{P196L}:GFP
433 degradation is slightly faster and more efficient than that of D14, the *35S:D14^{169E}:GFP;d14-1*
434 plants have a phenotype similar to *d14-1* of increased branching and reduced height
435 (Supplemental Fig. 1E, J, K) and a partial degradation of SMXL7 (Fig. 5A-C). The latter observation
436 also shows that SMXL7 degradation is in line with SL signalling and that an incomplete
437 degradation of SMXL7 is insufficient to achieve full SL signalling, at least in terms of the control
438 of branching patterns and plant height. However, D14 degradation does not provide information
439 about, nor is necessarily associated with the success of SL signalling.
440
441 *SL binding but not hydrolysis is required for D14 degradation*
442 D14 is an unusual hormone receptor that not only binds but also hydrolyses the bound SL
443 molecule. This has raised the question of whether binding is sufficient, or hydrolysis is also

444 required for SL signalling (Yao *et al.*, 2016; Saint Germain *et al.*, 2016; Seto *et al.*, 2019). Likewise,
445 it is yet unclear whether both binding and hydrolysis are needed for SL-induced D14
446 degradation. Rice transgenic lines expressing *D14* genes carrying mutations in the catalytic triad,
447 which preclude D14 from hydrolysing the SL ligand, showed a drastic decrease in D14
448 degradation (Hu *et al.*, 2017). This led to the proposal that hydrolysis was necessary for SL-
449 mediated destabilisation of D14.
450 Therefore, we assayed the stability of the $D14^{H247A}$ mutant that bears a histidine for alanine
451 substitution at the catalytic triad and has been suggested to be incapable to hydrolyse SLs (Yao
452 *et al.*, 2016). Time-lapse studies of *35S:D14^{H247A}:GFP;d14-1* transgenic lines showed that
453 $D14^{H247A}$:GFP was fully resistant to $GR24^{5DS}$-induced degradation *in planta* (Supplemental Fig. 6D,
454 E). Moreover, the *35S:D14^{H247A}:GFP;d14-1* lines had a strong *d14* mutant phenotype
455 (Supplemental Fig. 1C, H, K). However, more recently it has been shown that SL binding is also
456 impaired in $D14^{H247A}$ (Seto *et al.,* 2019). We confirmed this observation by DSF assays with
457 $GR24^{5DS}$ and $D14^{H247A}$:GFP, which showed no thermal shift (Supplemental Fig. 5A, C). These
458 results indicate that mutations at the catalytic triad of D14 can affect not only hydrolysis but
459 also hormone binding, and underscore the need for caution when interpreting the behaviour of
460 mutants in the catalytic triad of D14. In any case, this also confirms that SL binding is essential
461 for D14 degradation.
462
463 Therefore, instead of catalytic triad mutants, we used an alternative, pharmacological approach
464 to investigate the requirement for SL hydrolysis: a non-hydrolysable SL derivative, carba-GR24
465 (Thuring *et al.,* 1997; Prandi & McErlean, 2019). We performed LUC assays in *UB:D14:LUC* lines
466 treated with carba-GR24 or GR24, and found that D14:LUC was still degraded in the presence of
467 carba-GR24 (Fig. 6A, C) although at a slower rate and using higher concentrations of the
468 compound (20 µM) than when treated with GR24 (Fig. 6A, B). These results indicate that
469 hormone hydrolysis is not essential for D14 degradation, although it reduces protein half-life
470 during the process. Moreover, 20 µM carba-GR24 also promoted SMXL7:LUC degradation
471 although, at significantly slower rate and with lower efficiency (up to 45% of its original values)
472 than GR24 (Fig. 6D-F). Consistently, FRET assays showed that carba-GR24 enabled the
473 interaction of D14 with SMXL7 (Fig. 6G). These results suggest that D14 and SMXL7 degradation
474 (and probably SL signalling) can also occur without SL hydrolysis, although in a less efficient
475 manner.
476
477 **Discussion**

478 Extensive work performed in Arabidopsis and rice allowed the generation of a working model of
479 the molecular mechanisms controlling SL perception and signalling. Compelling evidence
480 indicates that D14 is the only receptor for the endogenous SLs, and that it also hydrolyses the
481 hormone. Moreover, the pivotal role of the SCF^{MAX2} complex in the ubiquitination and
482 proteasomal degradation of the transcriptional repressors SMXL6, SMXL7 and SMXL8 has been
483 largely proven. The observation that D14 is itself destabilised in the presence of SLs has raised
484 the question of whether a potential feedback regulatory mechanism of SL perception is
485 controlled by the same machinery that causes SMXLs degradation. Previous work has suggested
486 that this is the case (Chevalier *et al.,* 2014; Hu *et al.,* 2017), at least to a significant extent. Here
487 we present evidence of a more complex scenario in which, in addition to the SCF^{MAX2}-dependent
488 pathway of D14 degradation via the proteasome in Arabidopsis, alternative pathways may
489 contribute to limiting D14 protein levels in the presence of SLs.
490 Indeed, SCF^{MAX2} is not strictly required for SL-induced D14 degradation in Arabidopsis: in *max2*
491 mutants D14 gets destabilised, although less efficiently than in wild type. Moreover, D14 mutant
492 proteins predicted to be incapable of interacting with MAX2, namely $D14^{G158E}$ and $D14^{P169L}$ (Yao
493 *et al.,* 2016; Chevalier *et al.,* 2014), still display a significant degradation in response to SLs. This
494 indicates that alternative pathways exist, although not as effective as that of SCF^{MAX2}. Other E3
495 ligases could promote D14 degradation. For instance, a physical interaction has been reported
496 between rice D14 and the RING-finger ubiquitin E3 ligase SDEL1 under phosphate (Pi) deficiency,
497 which promotes degradation of SPX DOMAIN-CONTAINING PROTEIN 4 and release of
498 PHOSPHATE STARVATION RESPONSE PROTEIN 2, thus improving Pi acquisition and translocation
499 (Gu *et al.*, 2023). It remains to be tested whether D14 undergoes ubiquitination and degradation
500 in this system. Nevertheless, the MAX2-independent pathway of D14 degradation observed in
501 this work may not involve the proteasome, as the destabilisation of D14:GFP in *max2*, and that
502 of $D14^{G158E}$ and $D14^{P169L}$ are not blocked by proteasome inhibitors. Alternative proteolytic
503 pathways need to be explored to fully understand this phenomenon.
504 In addition, it has been proposed that the degradation of rice D14 is tightly coupled to the
505 degradation of D53, the rice ortholog of the SMXLs. This was based on the observation that
506 D14:GFP destabilisation is significantly impaired (although not abolished) in the SL-insensitive
507 *d53* mutants (Hu *et al.*, 2017). In Arabidopsis, we have found that D14 degradation is similar in
508 wild type and *smxl678* mutants, which indicates that lack of SMXLs does not influence D14
509 destabilisation. However, SMXLs may delay D14 degradation through the MAX2-independent
510 pathway, as inferred by the faster degradation of D14 in the *smxl678;max2* mutants than in the
511 *max2* mutants. Without a functional SCF^{MAX2}, the interaction of the SMXLs with SL-D14 could in
512 part protect D14 from the proteolytic machinery.

513 Furthermore, we have observed plants displaying, on one hand, an efficient wild type-like
514 degradation of SMXL7 together with a poor degradation of D14^{G158E} and, on the other hand, a
515 limited degradation of SMXL7 along with a fast and efficient degradation of D14^{P169L}. This
516 indicates that both responses are not always necessarily coupled in a quantitative manner. The
517 D14^{G158E} and D14^{P169L} mutants may be affected differently in the SL-induced conformational
518 changes of D14 (as DSF studies have shown for D14^{G158E}). This may impact their interactions with
519 the SMXLs and with the proteolytic machineries, thereby facilitating some responses and
520 preventing others.
521 Nevertheless, whereas SMXL7 degradation is strongly associated with the status of SL signalling,
522 D14 degradation does not seem to provide information about the success of SL signalling. This
523 is clearly illustrated by the fast-degrading D14^{P169L} mutant protein, which is unable to rescue the
524 *d14-1* phenotype (Chevalier *et al.,* 2014). Moreover, a partial degradation of SMXL7 (as observed
525 in *max2* mutants and in *35S:D14^{P169L}:GFP;d14-1* lines) is insufficient to achieve full SL signalling,
526 at least in terms of branching and height phenotypes.
527 The requirement of SL hydrolysis for the degradation of D14 was also an open question. Hu *et*
528 *al.* (2017) had shown that rice D14:GFP proteins carrying mutations in residues of the catalytic
529 triad essential for the hydrolase activity display severely impaired D14 degradation, which led
530 them to propose that hydrolysis is essential for this process. However, it is becoming increasingly
531 clear that some D14 catalytic triad mutants are unable to bind SLs (Zhao *et al.,* 2015; Seto *et al.,*
532 2019, this work), which highlights the importance of being cautious when interpreting results
533 regarding catalytic triad mutants. Our results demonstrate that the non-hydrolysable SL carba-
534 GR24 promotes degradation of D14, interaction between D14 and SMXL7, and destabilisation of
535 SMXL7. These findings strongly suggest that SL hydrolysis is not essential in this process, and are
536 in line with the proposal that the intact SL molecule serves as the active compound that triggers
537 conformational changes in D14 and initiates not only SL signalling (Seto *et al.,* 2019) but also D14
538 degradation.
539 Our studies with D14 mutant proteins also provide information about the functional domains of
540 the D14 protein and its interactions with other components of the SL signalling pathway. For
541 instance, the observation that in *35S:D14^{G158E}:GFP/+;UB:SMXL7:LUC/+;d14-1* plants, SMXL7:LUC
542 displays almost wild-type degradation dynamics suggests that the mutant protein D14^{G158E}:GFP
543 (unable to interact with D3/MAX2 ,Yao *et al.,* 2016), could still interact with SMXL7:LUC and
544 target it for degradation through a yet unknown but rather efficient mechanism.
545 D14^{P169L}, whose mutation is also located in the lid domain, has been proposed to fail to interact
546 with MAX2 (Chevalier *et al.*, 2014). Although our attempts to directly test D14 and MAX2
547 interactions using YTH and FRET assays were unsuccessful, the observation that D14^{P169L}:GFP

548 degradation dynamics are the same in wild type and *max2* mutants support the possibility of a
549 lack of interaction between $D14^{P169L}$ and MAX2. Remarkably, unlike $D14^{G158E}$, the $D14^{P169L}$ mutant
550 is very inefficient in targeting SMXL7:LUC for degradation. $D14^{P169L}$ seems to interact with other
551 SMXL proteins, perhaps with higher affinity than with SMXL7 (Li *et al.*, 2022). This might account
552 for the incomplete degradation of SMXL7:LUC and the pronounced mutant phenotype observed
553 in the mutant lines.
554 In conclusion, our investigation into the degradation patterns of wild-type and mutant D14
555 proteins *in planta* reveals novel regulatory features of SL-induced D14 destabilisation. Beyond
556 the canonical pathway involving ubiquitination by SCF^{MAX2} and subsequent proteasomal
557 degradation, our findings highlight the existence of additional mechanisms that operate
558 independently of MAX2 and the proteasomal machinery. Remarkably, these MAX2-independent
559 mechanisms can also effectively target SMXL7 for degradation. Moreover, SMXLs are not
560 required for SL-induced degradation of D14. Advanced and sensitive proteomic assays and
561 genetic analysis may help identify additional interactors of D14 involved in its destabilisation
562 upon SL binding. These new interactors may shed light on the crosstalk between SL signalling
563 and other signalling pathways, contributing to a more comprehensive view of the plant hormone
564 response networks.
565
566 **Acknowledgements**
567 The research was supported by grants from Spanish Ministry of Economy (MINECO) and fondos
568 FEDER PID2020-112779RB-I00/AEI/ 10.13039/501100011033, BIO2017-84363-R, BIO2017-
569 84066-R and BIO2014-57011-R]. Elena Sánchez Martín-Fontecha had an FPI (MINECO)
570 fellowship BES-2015-074233, funded by MCIN/AEI/10.13039/501100011033 and by ESF Invest
571 in Your Future.
572
573
574
575 **Author contributions**
576 PC designed research, ESMF and MB performed research, PC, ESMF, FC, MB and CP analysed
577 data, CP provided materials, PC, ESMF and FC wrote article.

578 **Figure legends**

579

580 **Fig. 1. D14:GFP and D14:LUC degradation in the presence of SL.**

581 (A) Time-lapse fluorescence study of D14:GFP signal decay (relative to mock treatment values)
582 of hypocotyls (H) and roots (R) of *35S:D14:GFP* seedlings in wild type (wt) and *d14-1* mutants
583 treated with 5 μM $GR24^{5DS}$ and/or the proteasome inhibitors (Inh.) 50 μM MG132 and 20 nM
584 epoxomicin. Solvents (acetone for $GR24^{5DS}$, DMSO for the inhibitors) were used as mock
585 treatments (n=4). (B-C) D14:GFP protein half-life (B) and endpoint signal at 16 h (C) calculated
586 from data in A. Square symbols represent hypocotyls, while triangles stand for roots. (D-E) LUC
587 assays of D14:LUC signal decay (relative to mock treatment values) of *UB:D14:LUC* (D) and
588 *UB:D14:LUC;d14-1* (E) seedlings in response to various concentrations of $GR24^{5DS}$ or acetone as
589 a mock treatment (n=6). (F-G) D14:LUC protein half-life (F) and endpoint signal at 15 h (G)
590 calculated from data in D and E. Data shown as mean ± SE. Symbols clipped at the edge of the Y
591 axis indicate conditions in which protein half-life is longer than 16 h (B) or 15 h (F). Different
592 letters denote statistical differences in one-way ANOVA with post hoc Tukey test, $P < 0.05$.

593

594 **Fig. 2. SL-induced D14:GFP degradation is only partly mediated by the 26S proteasome.**

595 (A) D14:GFP is poly-ubiquitinated in response to GR24. Seven dpg, *35S:D14:GFP* plants were
596 incubated with 10 μM GR24 and 50 μM MG132 for 3 h. Poly-ubiquitinated proteins were affinity
597 purified from protein extracts by incubation with Ub-binding p62 resin (+) or empty agarose
598 resin (negative control; −). Immunoblots were performed with α-ubiquitin antibodies to detect
599 total ubiquitinated proteins or α-GFP to detect D14:GFP and its ubiquitinated forms
600 (Ub(n):D14:GFP). The molecular mass of the D14:GFP protein is indicated. (B). Immunoblot of 7
601 dpg *35S:D14:GFP* seedlings treated for 8 h with 5 μM GR24 and the proteasome inhibitors
602 (Inhibitors) 50 μM MG132 and 20 nM epoxomicin. In the indicated lanes, 50 μM cycloheximide
603 (CHX) was added to prevent *de novo* protein synthesis. Solvents (acetone for GR24, DMSO for
604 CHX and Inhibitors) were used as mock treatments. An α-actin antibody was used for loading
605 control. The molecular masses of D14:GFP and actin are indicated.

606

607 **Fig 3. MAX2-independent D14 degradation.**

608 (A-D) Time-lapse fluorescence study of signal decay (relative to mock treatment values) of
609 hypocotyls (H) and roots (R) treated with 5 μM $GR24^{5DS}$ and/or the proteasome inhibitors (Inh.)
610 50 μM MG132 and 20 nM epoxomicin for D14:GFP (A), D14:GFP (*d14-1* background) (B),
611 D14:GFP (*max2-1* background) (C), $D14^{G158E}$:GFP (*d14-1* background) (D) and $D14^{P169L}$:GFP (*d14-*
612 *1* background) (E). Solvents (acetone for $GR24^{5DS}$, DMSO for the Inhibitors) were used as mock

613 treatments (n=3). (E-F) D14:GFP, D14^{G158E}:GFP and D14^{P169L}:GFP protein half-life (F) and endpoint
614 signal at 16 h (G) calculated from data in A-D. Square symbols represent hypocotyls, while
615 triangles stand for roots. (H) LUC assay of D14:LUC signal decay (relative to mock treatment
616 values) of *UB:D14:LUC* seedlings in wild type (wt) and *max2-1* mutants treated with 5 µM
617 GR24^{5DS} or acetone as mock control (n=6-9). (I-J) D14:LUC half-life (I) and endpoint signal at 15
618 h (J) calculated from data in H. Data shown as mean ± SE. Symbols clipped at the edge of the Y
619 axis (F, G) indicate conditions in which protein half-life is longer than 16 h or 15 h. Different
620 letters denote statistical differences in one-way ANOVA with post hoc Tukey test, $P < 0.05$;
621 asterisks indicate significant differences between pairs in Student's t test (**** $P < 0.0001$; ***
622 $P < 0.001$).
623
624 **Fig. 4. D14:LUC degradation does not require the SMXLs.**
625 (A) LUC assay of D14:LUC signal decay (relative to mock treatment values) of *UB:D14:LUC* in wild
626 type (wt), *max2-1*, *smxl6/7/8* triple mutant (*s678*) and *s678max2-1* (*s678m*) quadruple mutant
627 seedlings treated with 5 µM GR24^{5DS} or acetone as a mock control. (B-C) D14:LUC protein half-
628 life (B) and endpoint signal at 15 h (C) calculated from data in A. Data shown as mean ± SE (n=12).
629 Symbols clipped at the edge of the Y axis indicate conditions in which protein half-life is longer
630 than 15 h. Different letters denote statistical differences in one-way ANOVA with post hoc Tukey
631 test, $P < 0.05$.
632
633 **Fig. 5. Relationship between SL signalling and D14 degradation.**
634 (A) LUC assay of SMXL7:LUC signal decay (relative to mock treatment values) of *UB:SMXL7:LUC*
635 wild type (wt), *d14-1, max2-1, 35S:D14^{P169L}:GFP;d14-1* (D14^{P169L}) or *35S:D14^{G158E}:GFP;d14-1*
636 (D14^{G158E}) seedlings treated with 5 µM GR24^{5DS} or acetone as mock (n=6). SMXL7:LUC protein
637 half-life (B) and endpoint signal (C) at 3 h calculated from data in A. Data shown as mean ± SE.
638 (D) LUC assay of SMXL7:LUC signal decay (relative to mock treatment values) of *UB:SMXL7:LUC*
639 seedlings in response to various concentrations of GR24^{5DS} or acetone as a mock control (n=4).
640 SMXL7:LUC protein half-life (E) and endpoint signal (F) at 3 h calculated from data in D. In B and
641 E, symbols clipped at the edge of the Y axis indicate conditions in which protein half-life is longer
642 than 3 h. Different letters denote statistical differences in one-way ANOVA with post hoc Tukey
643 test, $P < 0.05$.
644
645 **Fig. 6. SL binding but not hydrolysis is necessary for D14 degradation.**
646 (A) LUC assays of D14:LUC signal decay (relative to mock treatment values) in *UB:D14:LUC*
647 seedlings treated with various concentrations of GR24^{5DS}, the non-hydrolysable SL carba-GR24,

648 or acetone (mock). (B-C) D14:LUC protein half-life (B) and endpoint signal at 15 h (C) calculated
649 from data in A (n=6). Symbols clipped at the edge of the Y axis indicate conditions in which
650 protein half-life is longer than 15 h. Different letters denote statistical differences in one-way
651 ANOVA with Welch'ś test. (D) LUC assay of SMXL7:LUC signal decay (relative to mock treatment
652 values) of *UB:SMXL7:LUC* seedlings in response to various concentrations of $GR24^{5DS}$, the non-
653 hydrolysable SL C.L. or acetone as mock (n=6). (E-F) SMXL7:LUC protein half-life (E) and endpoint
654 signal at 3 h (F) calculated from data in D. (D) FRET-APB of SMXL7:mCherry and D14:GFP after
655 30 min of treatment with 20 µM $GR24^{rac}$ or 50 µM C.L. E_{FRET}% is calculated as the relative increase
656 in GFP fluorescence intensity after photobleaching of the mCherry acceptor (n=6-12 nuclei).
657 Positive control, intramolecular FRET of a SMXL7:mCherry:GFP protein. Data shown as mean ±
658 SE. In B and E, symbols clipped at the edge of the Y axis indicate conditions in which protein half-
659 life is longer than 15 h or 3 h. Different letters denote statistical differences in one-way ANOVA
660 with post hoc Tukey test, $P < 0.05$; asterisks indicate significant differences between pairs in
661 Student's t test (**** p<0.0001; ** p<0.01).
662
663 **Supplemental Table S1. Primers used in this work**
664
665 **Supplemental Fig. 1. Functional analysis of D14:GFP, D14:LUC and D14:GFP mutant proteins.**
666 (A-J) Shoot branching (A-E) and height (F-J) phenotypes of wild type (wt), *d14-1* and
667 *35S:D14:GFP;d14-1* lines (A, F), *UB:D14:GFP;d14-1* lines (B, G), *35S:D14*^{H247A}*:GFP;d14-1* (C, H),
668 *35S:D14*^{G158E}*:GFP;d14-1* (D, I) and *35S:D14*^{P169L}*:GFP;d14-1* (E, J) two weeks after bolting.
669 Branching is denoted as the number of primary rosette branches/number of rosette leaves
670 (RI/RL). Violin plots represent data distribution. Black dotted lines indicate median values; grey
671 dotted lines delimit the interquartile range (n=11-16). (K) Images of representative individuals
672 from each line. Different letters denote statistical differences in one-way ANOVA with post hoc
673 Tukey test, $P < 0.05$. For assays with *35S:D14:GFP;d14-1,* line L18 was used.
674
675 **Supplemental Fig. 2. D14:GFP time-lapse assay in hypocotyls.**
676 Time series of fluorescence images of the hypocotyl of *35S:D14:GFP;d14-1* seedlings treated
677 with 5 µM $GR24^{5DS}$ (A) or acetone as mock treatment (B). Images were taken every 20 minutes
678 up to 16 hours. Scale bar = 500 µm.
679
680 **Supplemental Fig. 3. D14:GFP time-lapse assay in roots.**

681 Time series of fluorescence images of the root of *35S:D14:GFP;d14-1* seedlings treated with 5
682 µM $GR24^{5DS}$ (A) or acetone as mock treatment (B). Images were taken every 20 minutes up to
683 16 hours. Scale bar = 500 µm
684
685 **Supplemental Fig. 4**. **Localization of the G158 and P169 residues possibly involved in the D14-**
686 **MAX2 interaction.** 3D molecular visualisation as a surface representation of the D14 protein in
687 modified PDB:4IH4 (Zhao *et al.*, 2013) (A,C) and PDB:5HZG (Yao *et al.*, 2016) (B,D). The α/β
688 hydrolase core domain is coloured in grey; the lid domain in salmon; residues of the catalytic
689 triad in blue; residues G158 and P169 are highlighted in red. In B and D, the ribbon
690 representation of the rice MAX2 orthologue OsD3 is coloured in green.
691
692 **Supplemental Fig. 6. Evaluation of D14, $D14^{H247A}$ and $D14^{G158E}$ protein stability in the presence**
693 **of $GR24^{5DS}$**. In the DSF assays, the melting temperature (Tm) profiles of the D14 (A), $D14^{G158E}$ (B)
694 and $D14^{H247A}$ (C) proteins, each isolated from *E. coli*, were monitored under increasing
695 concentrations of $GR24^{5DS}$, and thermal denaturation shifts observed in these proteins were
696 recorded.
697
698 **Supplemental Fig. 5. Analysis of $D14^{H247A}$:GFP and $D14^{G158E}$:GFP stability in response to $GR24^{5DS}$.**
699 (A) Time-lapse fluorescence study of $D14^{P169L}$:GFP signal decay (relative to mock treatment
700 values) of hypocotyls (H) and roots (R) of *35S:D14^{P169L}:GFP;d14-1* seedlings treated with 5 µM
701 $GR24^{5DS}$ or acetone (mock). (B-C) $D14^{P169L}$:GFP protein half-life (B) and endpoint signal at 16 h
702 (C) calculated from data in A. Square symbols represent hypocotyls, while triangles stand for
703 roots. (D) Time-lapse fluorescence study of $D14^{H247A}$:GFP signal decay (relative to mock
704 treatment values) of hypocotyls (H) and roots (R) of *35S:D14^{H247A}:GFP;d14-1* seedlings treated
705 with 5 µM $GR24^{5DS}$ or acetone (mock). (E) $D14^{H247A}$:GFP endpoint signal at 16 h calculated from
706 data in D. Square symbols represent hypocotyls; triangles, roots. Data shown as mean ± SE (n=3).
707 In B, symbols clipped at the edge of the Y axis indicate conditions in which protein half-life is
708 longer than 16 h. Different letters denote statistical differences in one-way ANOVA with post
709 hoc Tukey test, $P < 0.05$.
710
711 **Supplemental File S1. D14:GFP time-lapse assay in hypocotyls**.
712
713 **Supplemental File S2. D14:GFP time-lapse assays in roots.**
714

Akiyama K, Matsuzaki KI, Hayashi H. 2005. Plant sesquiterpenes induce hyphal branching in arbuscular mycorrhizal fungi. Nature **435**, 824–827.

Al-Babili S, Bouwmeester HJ. 2015. Strigolactones, a Novel Carotenoid-Derived Plant Hormone. Annual Review of Plant Biology **66**, 161–186.

Arite T, Umehara M, Ishikawa S, Hanada A, Maekawa M, Yamaguchi S, Kyozuka J. 2009. d14, a strigolactone-insensitive mutant of rice, shows an accelerated outgrowth of tillers. Plant & cell physiology **50**, 1416–1424.

Barbier F, Fichtner F, & Beveridge C. 2023. The strigolactone pathway plays a crucial role in integrating metabolic and nutritional signals in plants. Nature Plants **9**, 1191–1200.

Besserer A, Puech-Pagès V, Kiefer P, Gomez-Roldan V, Jauneau A, Roy S, Portais J-C, Roux C, Bécard G, Séjalon-Delmas N. 2006. Strigolactones Stimulate Arbuscular Mycorrhizal Fungi by Activating Mitochondria. (J Chory, Ed.). PLoS Biology **4**, e226.

Blázquez MA, Nelson DC, Weijers D. 2020. Evolution of Plant Hormone Response Pathways. Annual Review of Plant Biology **71**, 327–353.

Bleckmann A, Weidtkamp-Peters S, Seidel CAM, Simon R. 2010. Stem cell signalling in Arabidopsis requires CRN to localize CLV2 to the plasma membrane. Plant physiology **152**, 166–176.

Brewer PB, Yoneyama K, Filardo F, *et al.* 2016. LATERAL BRANCHING OXIDOREDUCTASE acts in the final stages of strigolactone biosynthesis in Arabidopsis. Proceedings of the National Academy of Sciences **113**, 6301–6306.

Bürger M, Mashiguchi K, Lee HJ, Nakano M, Takemoto K, Seto Y, Yamaguchi S, Chory J. 2019. Structural Basis of Karrikin and Non-natural Strigolactone Perception in Physcomitrella patens. Cell reports **26**, 855-865.e5.

Chevalier F, Nieminen K, Sánchez-Ferrero JC, Rodríguez ML, Chagoyen M, Hardtke CS, Cubas P. 2014. Strigolactone promotes degradation of DWARF14, an α/β hydrolase essential for strigolactone signalling in Arabidopsis. The Plant Cell **26**, 1134–1150.

Clough SJ, Bent AF. 1998. Floral dip: a simplified method for Agrobacterium-mediated transformation of Arabidopsis thaliana. The Plant journal : for cell and molecular biology **16**, 735–743.

Flematti GR, Scaffidi A, Waters MT, Smith SM. 2016. Stereospecificity in strigolactone biosynthesis and perception. Planta **243**, 1361–1373.

Fox J. 2005. The R Commander: A Basic-Statistics Graphical User Interface to R. Journal of Statistical Software **14**, 1–42.

Gu P, Tao W, Tao J, *et al.* 2023. The <scp>D14-SDEL1-SPX4</scp> cascade integrates the strigolactone and phosphate signalling networks in rice. New Phytologist **239**, 673–686.

Hu Q, He Y, Wang L, *et al.* 2017. DWARF14, A Receptor Covalently Linked with the Active Form of Strigolactones, Undergoes Strigolactone-Dependent Degradation in Rice. Frontiers in Plant Science **8**, 1935.

Ishikawa S, Maekawa M, Arite T, Onishi K, Takamure I, Kyozuka J. 2005. Suppression of Tiller Bud Activity in Tillering Dwarf Mutants of Rice. Plant and Cell Physiology **46**, 79–86.

Jiang L, Liu X, Xiong G, *et al.* 2013. DWARF 53 acts as a repressor of strigolactone signalling in rice. Nature **504**, 401–405.

Johnson X, Brcich T, Dun EA, Goussot M, Haurogné K, Beveridge CA, Rameau C. 2006. Branching genes are conserved across species. Genes controlling a novel signal in pea are coregulated by other long-distance signals. Plant physiology **142**, 1014–1026.

Karimi M, De Meyer B, Hilson P. 2005. Modular cloning in plant cells. Trends in Plant Science **10**, 103–105.

Lanfranco L, Fiorilli V, Venice F, Bonfante P. 2018. Strigolactones cross the kingdoms: plants, fungi, and bacteria in the arbuscular mycorrhizal symbiosis Journal of Experimental Botany **69**, 2175–2188.

765 **Liang Y, Ward S, Li P, Bennett T, Leyser O**. 2016. SMAX1-LIKE7 Signals from the Nucleus to
766 Regulate Shoot Development in Arabidopsis via Partially EAR Motif-Independent Mechanisms.
767 The Plant cell **28**, 1581–601.
768 **Li Q, Martín-Fontecha ES, Khosla A, White ARF, Chang S, Cubas P, Nelson DC**. 2022. The
769 strigolactone receptor D14 targets SMAX1 for degradation in response to GR24 treatment and
770 osmotic stress. Plant Communications **3**, 100303.
771 **Nakagawa T, Kurose T, Hino T, Tanaka K, Kawamukai M, Niwa Y, Toyooka K, Matsuoka K,**
772 **Jinbo T, Kimura T**. 2007. Development of series of gateway binary vectors, pGWBs, for
773 realizing efficient construction of fusion genes for plant transformation. Journal of bioscience
774 and bioengineering **104**, 34–41.
775 **Nicolas M, Rodríguez-Buey ML, Franco-Zorrilla JM, Cubas P**. 2015. A Recently Evolved
776 Alternative Splice Site in the BRANCHED1a Gene Controls Potato Plant Architecture. Current
777 Biology **25**, 1799–1809.
778 **Patil SB, Barbier FF, Zhao J, *et al.*** 2022. Sucrose promotes D53 accumulation and tillering in
779 rice. New Phytologist **234**, 122–136.
780 **Prandi C, McErlean CS.** 2019. The chemistry of strigolactones. Strigolactones-Biology and
781 Applications, Springer International Publishing, 163-198.
782 **Rameau C, Goormachtig S, Cardinale F, Bennett T, Cubas P**. 2019. Strigolactones as Plant
783 Hormones. Strigolactones - Biology and Applications. Springer International Publishing, 47–87.
784 **Ryun Woo H, Min Chung K, Park J-H, Aeong Oh S, Ahn T, Hyum Hong S, Key Jang S, Gil Nam H**.
785 2001. ORE9, an F-Box Protein That Regulates Leaf Senescence in Arabidopsis. The Plant Cell **13**,
786 1779–1790.
787 **de Saint Germain A, Clavé G, Badet-Denisot M-A, *et al.*** 2016. An histidine covalent receptor
788 and butenolide complex mediates strigolactone perception. Nature Chemical Biology **12**, 787–
789 794.
790 **Sánchez E, Artuso E, Lombardi C, *et al.*** 2018. Structure–activity relationships of strigolactones
791 via a novel, quantitative in planta bioassay. Journal of Experimental Botany **69**, 2333–2343.
792 **Sánchez E, Cubas P, Cardinale F, Visentin I**. 2021. Evaluation of bioactivity of strigolactone-
793 related molecules by a quantitative luminometer bioassay. Methods in Molecular Biology
794 **2309**, 191–200.
795 **Schindelin J, Arganda-Carreras I, Frise E, *et al.*** 2012. Fiji: an open-source platform for
796 biological-image analysis. Nature methods **9**, 676–82.
797 **Seto Y, Yasui R, Kameoka H, *et al.*** 2019. Strigolactone perception and deactivation by a
798 hydrolase receptor DWARF14. Nature Communications **10**, 191.
799 **Shabek N, Ticchiarelli F, Mao H, Hinds TR, Leyser O, Zheng N**. 2018. Structural plasticity of D3–
800 D14 ubiquitin ligase in strigolactone signalling. Nature **563**, 652–656.
801 **Soundappan I, Bennett T, Morffy N, Liang Y, Stanga JP, Abbas A, Leyser O, Nelson DC**. 2015.
802 SMAX1-LIKE/D53 Family members enable distinct MAX2-dependent responses to
803 strigolactones and karrikins in Arabidopsis. The Plant Cell **27**, 3143–3159.
804 **Stirnberg P, Furner IJ, Ottoline Leyser HM**. 2007. MAX2 participates in an SCF complex which
805 acts locally at the node to suppress shoot branching. The Plant journal : for cell and molecular
806 biology **50**, 80–94.
807 **Stirnberg P, van De Sande K, Leyser HMO**. 2002. MAX1 and MAX2 control shoot lateral
808 branching in Arabidopsis. Development (Cambridge, England) **129**, 1131–1141.
809 **Tal L, Palayam M, Ron M, Young A, Britt A, Shabek N**. 2022. A conformational switch in the
810 SCF-D3/MAX2 ubiquitin ligase facilitates strigolactone signalling. Nature Plants 8:5 **8**, 561–573.
811 **The R Development Core Team**. R: A Language and Environment for Statistical Computing. *in*
812 *press*.
813 **Thuring, JWJF, Nefkens GHL, and Zwanenburg B**. 1997. Synthesis and biological evaluation of
814 the strigol analogue carba-GR24. Journal of Agricultural and Food Chemistry **45**, 1409-1414.

Trasoletti M, Visentin I, Campo E, Schubert A, Cardinale F. 2022. Strigolactones as a hormonal hub for the acclimation and priming to environmental stress in plants. Plant Cell Environment. **45**, 3611–3630

Wang L, Wang B, Jiang L, Liu X, Li X, Lu Z, Meng X, Wang Y, Smith SM, Li J. 2015. Strigolactone signalling in Arabidopsis regulates shoot development by targeting D53-like SMXL repressor proteins for ubiquitination and degradation. The Plant Cell **27**, 3128–3142.

Yao R, Ming Z, Yan L, *et al.* 2016. DWARF14 is a non-canonical hormone receptor for strigolactone. Nature **536**, 469–473.

Yoneyama K, Xie X, Yoneyama K, Kisugi T, Nomura T, Nakatani Y, Akiyama K, McErlean CSP. 2018. Which are the major players, canonical or non-canonical strigolactones? Journal of Experimental Botany **69**, 2231–2239.

Zhao L-H, Zhou XE, Wu Z-S, *et al.* 2013. Crystal structures of two phytohormone signal-transducing α/β hydrolases: karrikin-signalling KAI2 and strigolactone-signalling DWARF14. Cell research **23**, 436–9.

Zhao L-H, Zhou XE, Yi W, *et al.* 2015. Destabilisation of strigolactone receptor DWARF14 by binding of ligand and E3-ligase signalling effector DWARF3. Cell Research **25**, 1219–1236.

Zhou F, Lin Q, Zhu L, *et al.* 2013. D14-SCF(D3)-dependent degradation of D53 regulates strigolactone signalling. Nature **504**, 406–10.

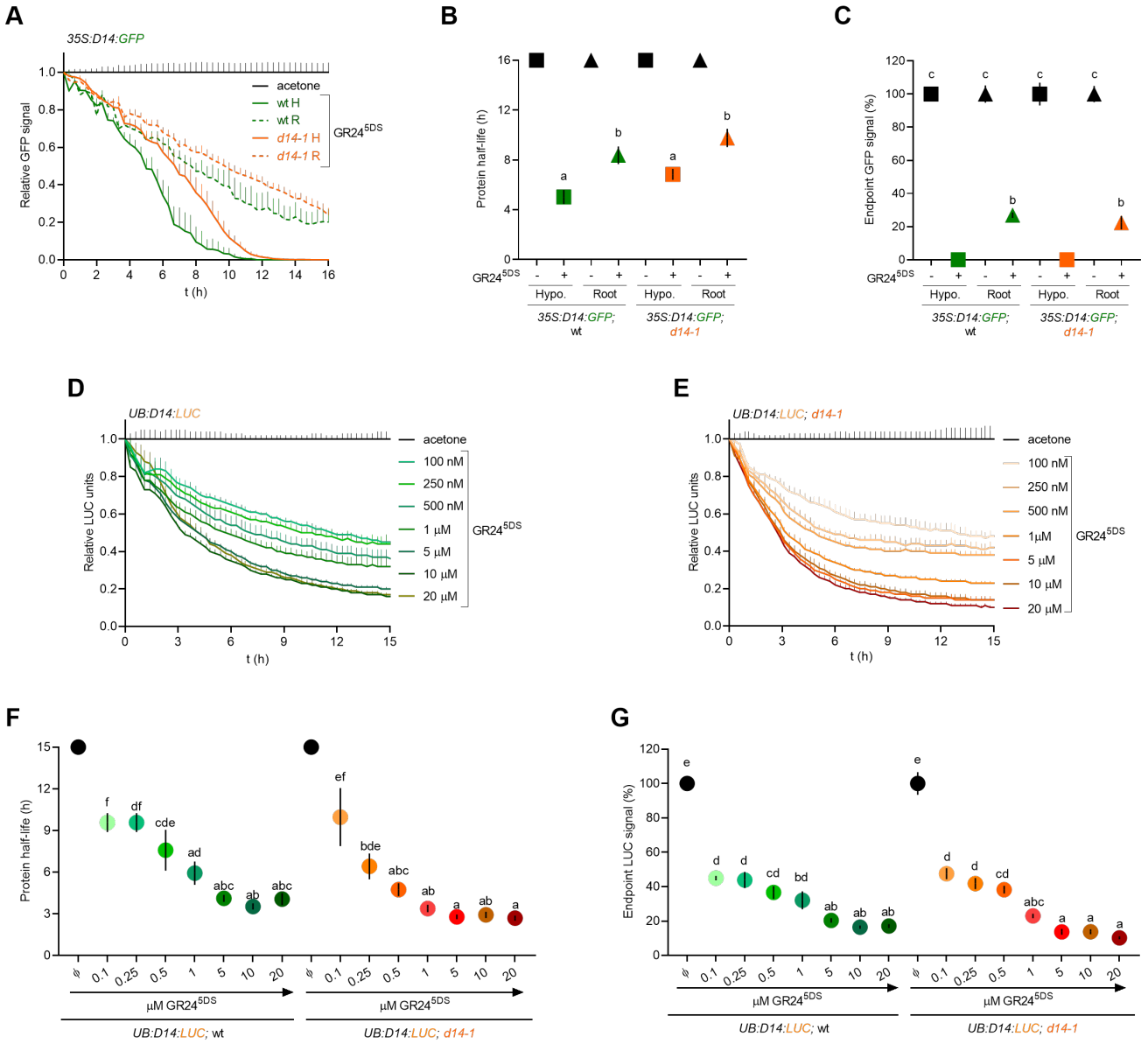

Fig. 1. D14:GFP and D14:LUC degradation in the presence of SL. (A) Time-lapse fluorescence study of D14:GFP signal decay (relative to mock treatment values) of hypocotyls (H) and roots (R) of *35S:D14:GFP* seedlings in wild type (wt) and *d14-1* mutants treated with 5 µM $GR24^{5DS}$ and/or the proteasome inhibitors (Inh.) 50 µM MG132 and 20 nM epoxomicin. Solvents (acetone for $GR24^{5DS}$, DMSO for the Inhibitors) were used as mock treatments (n=4). (B-C) D14:GFP protein half-life (B) and endpoint signal at 16 h (C) calculated from data in A. Square symbols represent hypocotyls, while triangles stand for roots. (D-E) LUC assays of D14:LUC signal decay (relative to mock treatment values) of *UB:D14:LUC* (D) and *UB:D14:LUC;d14-1* (E) seedlings in response to various concentrations of $GR24^{5DS}$ or acetone as a mock treatment (n=6). (F-G) D14:LUC protein half-life (F) and endpoint signal at 15 h (G) calculated from data in D and E. Data shown as mean ± SE. Symbols clipped at the edge of the Y axis indicate conditions in which protein half-life is longer than 16 h (B) or 15 h (F). Different letters denote statistical differences in one-way ANOVA with post hoc Tukey test, $P < 0.05$.

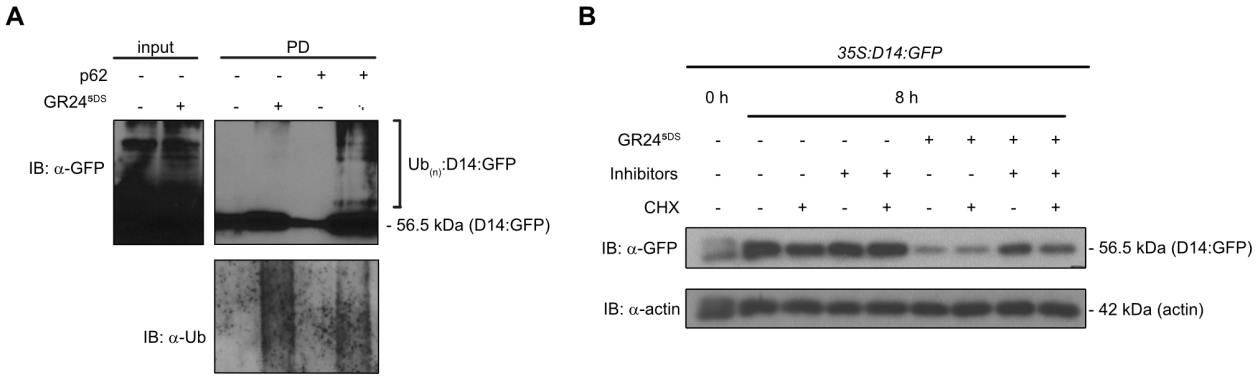

Fig. 2. SL-induced D14:GFP degradation is only partly mediated by the 26S proteasome. (A) D14:GFP is poly-ubiquitinated in response to GR24. Seven dpg, *35S:D14:GFP* plants were incubated with 10 μM GR24 and 50 μM MG132 for 3 h. Poly-ubiquitinated proteins were affinity purified from protein extracts by incubation with Ub-binding p62 resin (+) or empty agarose resin (negative control; –). Immunoblots were performed with α-ubiquitin antibodies to detect total ubiquitinated proteins or α-GFP to detect D14:GFP and its ubiquitinated forms (Ub(n):D14:GFP). The molecular mass of the D14:GFP protein is indicated. (B). Immunoblot of 7 dpg *35S:D14:GFP* seedlings treated for 8 h with 5 μM GR24 and the proteasome inhibitors (Inhibitors) 50 μM MG132 and 20 nM epoxomicin. In the indicated lanes, 50 μM cycloheximide (CHX) was added to prevent de novo protein synthesis. Solvents (acetone for GR24, DMSO for CHX and Inhibitors) were used as mock treatments. An α-actin antibody was used for loading control. The molecular masses of D14:GFP and actin are indicated.

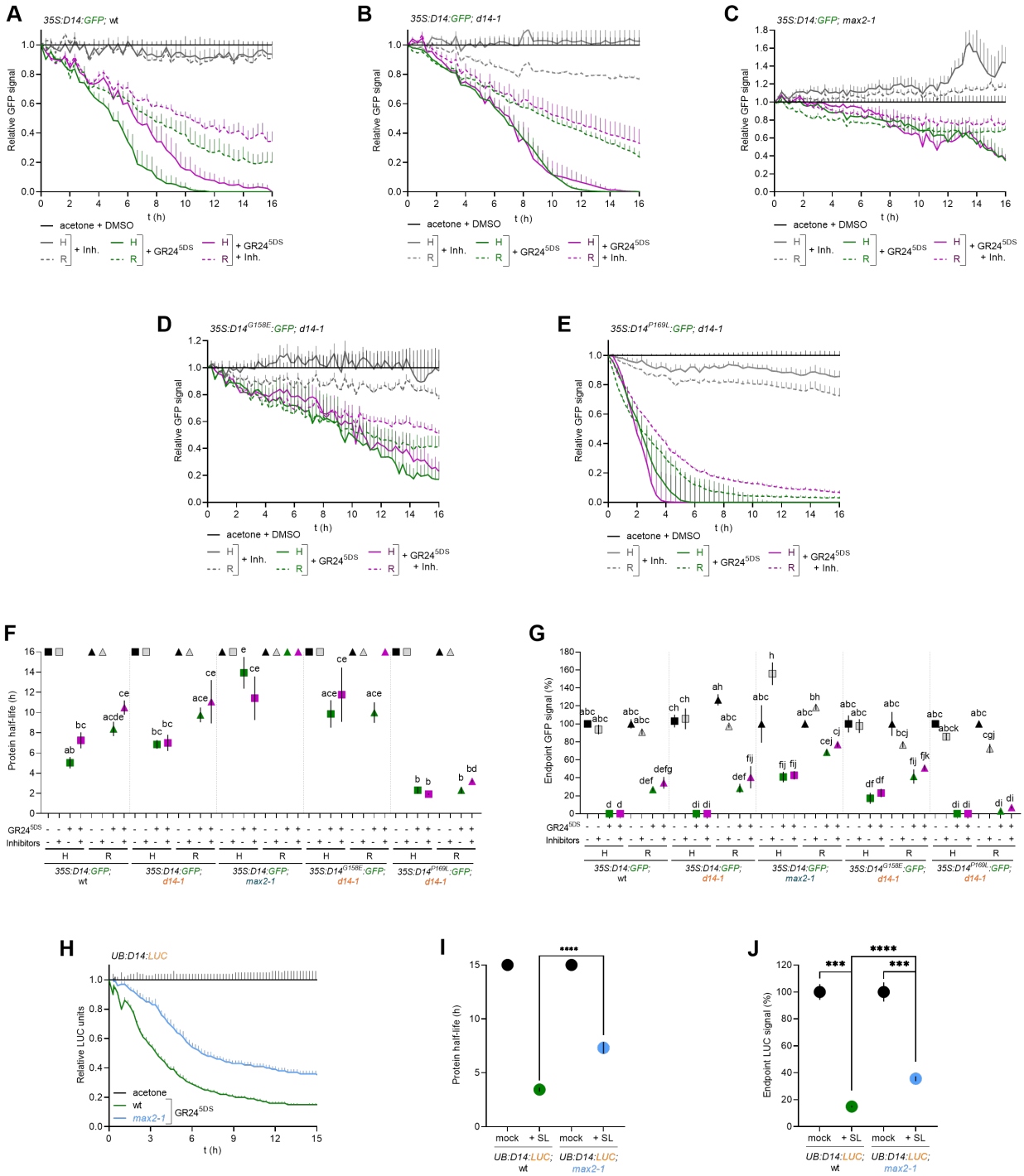

Fig 3. MAX2-independent D14 degradation. (A-D) Time-lapse fluorescence study of signal decay (relative to mock treatment values) of hypocotyls (H) and roots (R) treated with 5 µM $GR24^{5DS}$ and/or the proteasome inhibitors (Inh.) 50 µM MG132 and 20 nM epoxomicin for D14:GFP (A), D14:GFP (d14-1 background) (B), D14:GFP (max2-1 background) (C), $D14^{G158E}$:GFP (d14-1 background) (D) and $D14^{P169L}$:GFP (d14-1 background) (E). Solvents (acetone for $GR24^{5DS}$, DMSO for the Inhibitors) were used as mock treatments (n=3). (E-F) D14:GFP, $D14^{G158E}$:GFP and $D14^{P169}$L:GFP protein half-life (F) and endpoint signal at 16 h (G) calculated from data in A-D. Square symbols represent hypocotyls, while triangles stand for roots. (H) LUC assay of D14:LUC signal decay (relative to mock treatment values) of *UB:D14:LUC* seedlings in wild type (wt) and *max2-1* mutants treated with 5 µM $GR24^{5DS}$ or acetone as mock control (n=6-9). (I-J) D14:LUC half-life (I) and endpoint signal at 15 h (J) calculated from data in H. Data shown as mean ± SE. Symbols clipped at the edge of the Y axis (F, G) indicate conditions in which protein half-life is longer than 16 h or 15 h. Different letters denote statistical differences in one-way ANOVA with post hoc Tukey test, $P < 0.05$; asterisks indicate significant differences between pairs in Student's t test (**** $P < 0.0001$; *** $P < 0.001$).

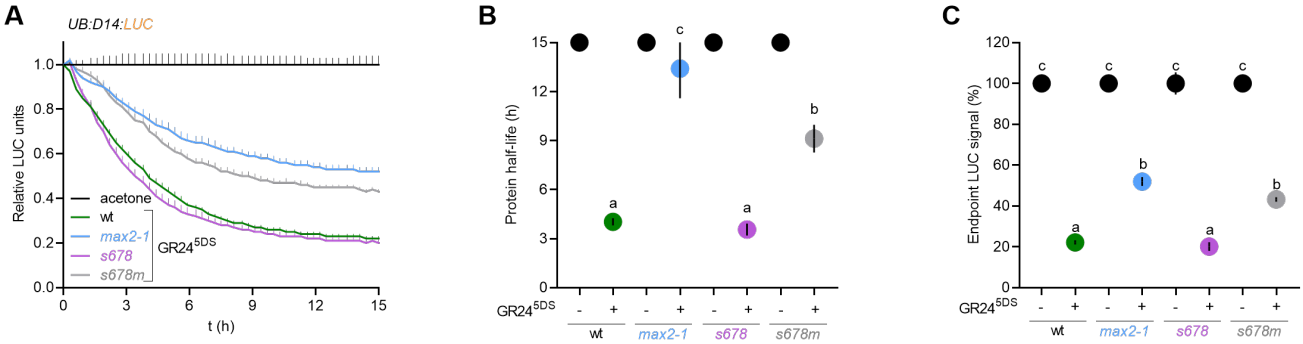

Fig. 4. D14:LUC degradation does not require the SMXLs. (A) LUC assay of D14:LUC signal decay (relative to mock treatment values) of *UB:D14:LUC* in wild type (wt), *max2-1*, *smxl6/7/8* triple mutant (*s678*) and *s678max2-1* (*s678m*) quadruple mutant seedlings treated with 5 µM GR24^{5DS} or acetone as a mock control. (B-C) D14:LUC protein half-life (B) and endpoint signal at 15 h (C) calculated from data in A. Data shown as mean ± SE (n=12). Symbols clipped at the edge of the Y axis indicate conditions in which protein half-life is longer than 15 h. Different letters denote statistical differences in one-way ANOVA with post hoc Tukey test, $P < 0.05$.

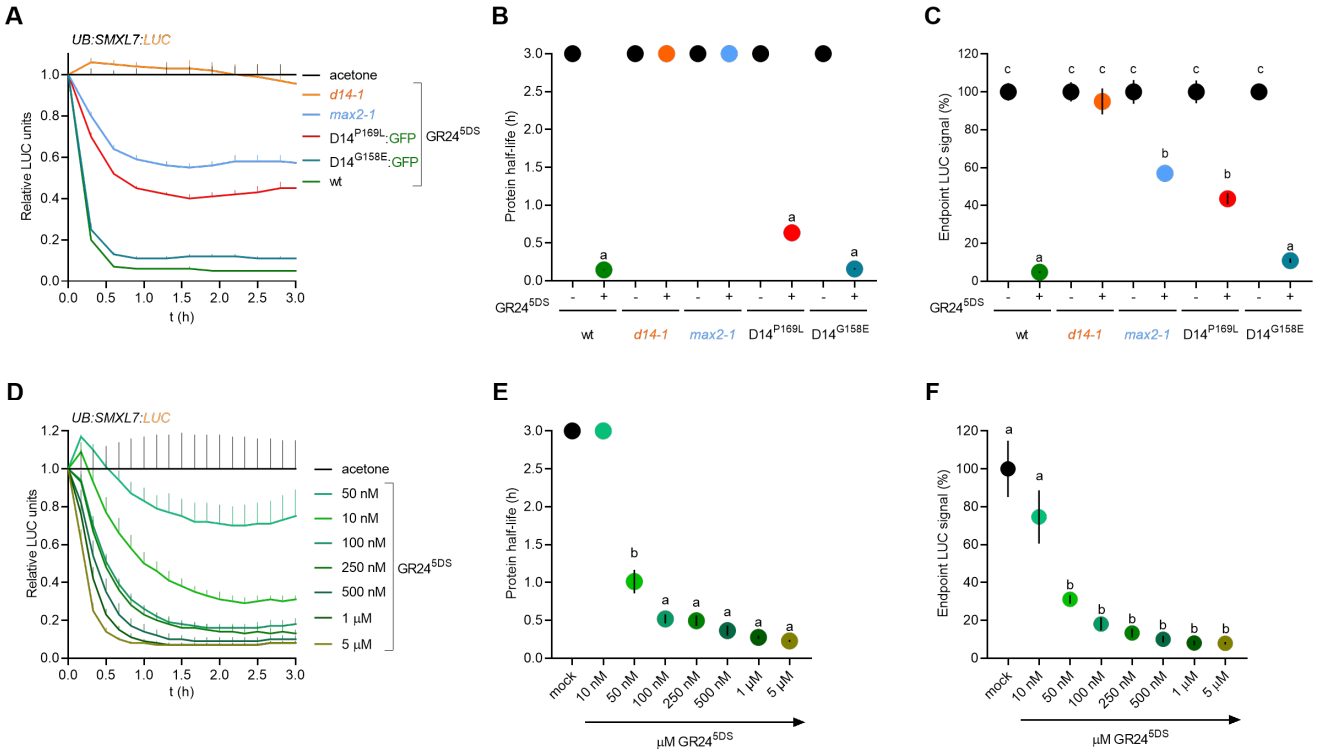

Fig. 5. SMXL7:LUC degradation in response to SL treatments. (A) LUC assay of SMXL7:LUC signal decay (relative to mock treatment values) of *UB:SMXL7:LUC* wild type (wt), d14-1, *max2-1*, *35S:D14^{G158E}:GFP;d14-1* (D14^{G158E}) or *35S:D14^{P169L}:GFP;d14-1* (D14^{P169L}) seedlings treated with 5 µM GR24^{5DS} or acetone as mock (n=6). SMXL7:LUC protein half-life (B) and endpoint signal (C) at 3 h calculated from data in A. Data shown as mean ± SE. (D) LUC assay of SMXL7:LUC signal decay (relative to mock treatment values) of *UB:SMXL7:LUC* seedlings in response to various concentrations of GR24^{5DS} or acetone as a mock control (n=4). SMXL7:LUC protein half-life (E) and endpoint signal (F) at 3 h calculated from data in D. In B and E, symbols clipped at the edge of the Y axis indicate conditions in which protein half-life is longer than 3 h. Different letters denote statistical differences in one-way ANOVA with post hoc Tukey test, $P < 0.05$.

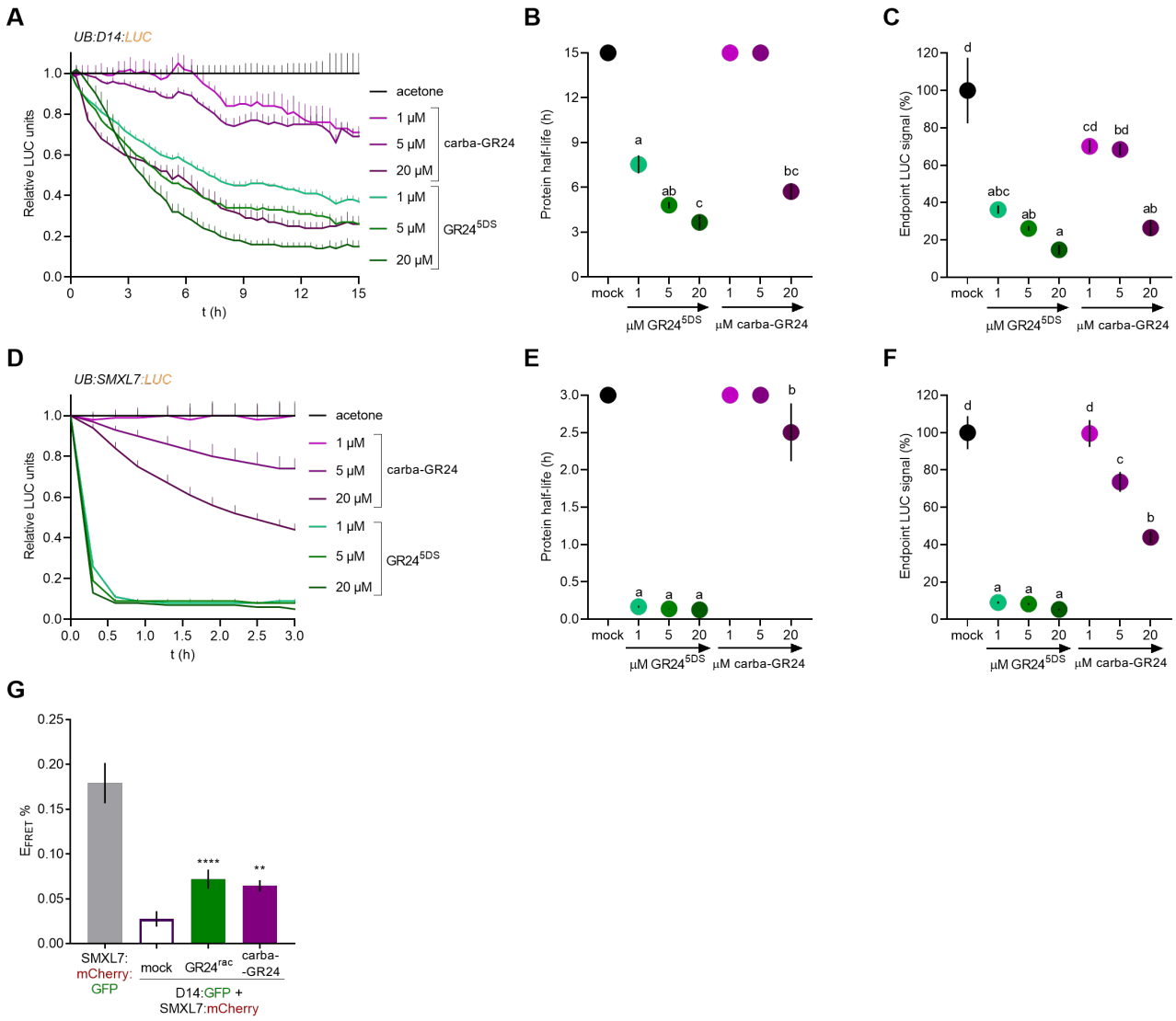

Fig. 6. SL binding but not hydrolysis is necessary for D14 degradation. (A) LUC assays of D14:LUC signal decay (relative to mock treatment values) in UB:D14:LUC seedlings treated with various concentrations of $GR24^{5DS}$, the non-hydrolysable SL carba-GR24, or acetone (mock). (B-C) D14:LUC protein half-life (B) and endpoint signal at 15 h (C) calculated from data in A (n=6). Symbols clipped at the edge of the Y axis indicate conditions in which protein half-life is longer than 15 h. Different letters denote statistical differences in one-way ANOVA with Welch´s test. (D) LUC assay of SMXL7:LUC signal decay (relative to mock treatment values) of *UB:SMXL7:LUC* seedlings in response to various concentrations of $GR24^{5DS}$, the non-hydrolysable SL carba-GR24 or acetone as mock (n=6). (E-F) SMXL7:LUC protein half-life (E) and endpoint signal at 3 h (F) calculated from data in D. (D) FRET-APB of SMXL7:mCherry and D14:GFP after 30 min of treatment with 20 µM $GR24^{rac}$ or 50 µM carba-GR24 EFRET% is calculated as the relative increase in GFP fluorescence intensity after photobleaching of the mCherry acceptor (n=6-12 nuclei). Positive control, intramolecular FRET of a SMXL7:mCherry:GFP protein. Data shown as mean ± SE. In B and E, symbols clipped at the edge of the Y axis indicate conditions in which protein half-life is longer than 15 h or 3 h. Different letters denote statistical differences in one-way ANOVA with post hoc Tukey test, $P < 0.05$; asterisks indicate significant differences between pairs in Student's t test (**** $p<0.0001$; ** $p<0.01$).